Blood Flow *in silico*: From Single Cells to Blood Rheology

Dmitry A. FEDOSOV[1], Julia FORNLEITNER[1], J. Liam McWHIRTER[1], Kathrin MÜLLER[1], Hiroshi NOGUCHI[1,2], Matti PELTOMÄKI[1], Gerhard GOMPPER[1*]

1: Theoretical Soft Matter and Biophysics, Institute of Complex Systems and Institute for Advanced Simulation, Forschungszentrum Jülich, 52425 Jülich, Germany
2: Institute for Solid State Physics, University of Tokyo, Chiba 277-8581, Japan
* Corresponding author: Tel.: +49 (0)2461 614012; Fax: +49 (0)2461 613180;
Email: g.gompper@fz-juelich.de

Abstract Mesoscale hydrodynamics simulations of red blood cells under flow have provided much new insight into their shapes and dynamics in microchannel flow. The presented results range from the behavior of single cells in confinement and the shape changes in sedimentation, to the clustering and arrangement of many cells in microchannels and the viscosity of red blood cell suspensions under shear flow. The interaction of red blood cells with other particles and cells, such as white blood cells, platelets, and drug carriers, shows an essential role of red blood cells in the margination of other blood components.

Keywords: Blood flow, blood cells, microchannels, mesoscale hydrodynamics, blood rheology, red blood cells, white blood cells, drug carriers, viscosity, sedimentation

1 Introduction

The flow behavior of vesicles and blood cells is important in many applications in biology and medicine. For example, the flow properties of blood in micro-vessels is determined by the rheological properties of red blood cells (RBCs). Blood flow is therefore strongly affected by diseases such as malaria or diabetes, where RBC deformability is strongly reduced. Furthermore, microfluidic devices have been developed recently, which allow the manipulation of small amounts of suspensions of particles or cells. This allows detailed experimental investigations of the structure and dynamics of single RBCs, but also of the arrangement of many RBCs, and their interactions with other blood components. Simulations of blood cells under flow play an important role to understand their structural and dynamical properties, and to predict their behavior under microfluidic flow conditions (Fedosov et al., 2014a). We present here a short overview of some of our recent simulation results.

2 Results

Of fundamental interest is the relation between the flow behavior and the elasticity and deformability of the blood cells, their long-range hydrodynamic interactions in microchannels, and thermal membrane undulations (Fedosov et al., 2014a). We study these mechanisms by a combination of particle-based mesoscale simulation techniques for the fluid hydrodynamics (Espanol and Warren, 1995; Espanol and Revenga, 2003; Kapral, 2008; Gompper et al., 2009) with triangulated-surface models for the membrane (Gompper and Kroll, 1997, 2004; Noguchi and Gompper, 2005; Fedosov et al., 2010). The essential control parameters are the volume fraction of RBCs (tube hematocrit H_t), the flow velocity v_0 or the shear rate $\dot{\gamma}$, and the capillary radius R_{cap}.

We present the results usually in dimensionless quantities or parameters, such as the confinement $\chi = R_0/R_{cap}$ (where R_0 is the average radius of an RBC as obtained from a sphere of equal surface area), and the dimensionless shear rate $\dot{\gamma}^* = \dot{\gamma}\tau$, where $\tau = \eta R_0^3/\kappa$ is a character-

istic RBC relaxation time in equilibrium (with fluid viscosity η and membrane bending rigidity κ). Since in simulations, pressure-driven flow in a capillary is conveniently generated by a uniform "gravitational" acceleration g, we also employ $g^* = \rho g R_0^4/k_B T$ to characterize fluid flow (with fluid mass density ρ); in the absence of RBCs, this corresponds to an average flow velocity $v_0 = \rho g R_{cap}^2/8\eta$.

2.1 Single Red Blood Cells in Microchannel Flows

Experimentally, RBCs are known to form bullet and parachute shapes in flow through microvessels or microcapillaries with diameters in the range from about 3 to 13 μm (Skalak, 1969; Secomb et al., 1986; Skalak, 1990; Suzuki et al., 1996). This behavior is well captured in simulations (Noguchi and Gompper, 2005; Fedosov et al., 2014b), where a single red blood cell in capillary flow shows a transition from the biconcave disk shape at low flow velocities to a parachute shape at high flow velocities, see Fig. 1. The simulations predict that the discocyte moves with its short axis *perpendicular* to the cylinder axis (Noguchi and Gompper, 2005).

An interesting question is here whether other shapes, such as the asymmetric slipper shape, which are often observed experientally (Abkarian et al., 2008; Tomaiuolo et al., 2009), are stationary states in capillary flow, or just appear as transient conformations. Simulations in two spatial dimensions (in which the RBC membrane is a closed line) indicate that slippers do exist as stable stationary shape for sufficiently small flow velocities, at least in the absence of thermal fluctuations (Kaoui et al., 2009, 2011).

Simulations in two spatial dimensions have the advantage that they are computationally much less demanding, so that state diagrams as a function of two or more parameters can be mapped out relatively easily. However, quantitative and sometimes qualitative predictions are only possible from full three-dimensional models and simulations. Our simulation results for three-dimensional systems (Fedosov et al., 2014b) are displayed in Figs. 1 and 2. Slipper shapes are indeed found to intervene between discocytes and parachutes; they are significant for relatively weak confinements of $\chi \lesssim 0.6$, while parachutes prevail for strong confinement. In addition, tumbling discocytes appear at weak confinement; this dynamic state occurs due to the shear modulus originating from the spectrin network of the RBC, an effect which can only be described in a three-dimensional model.

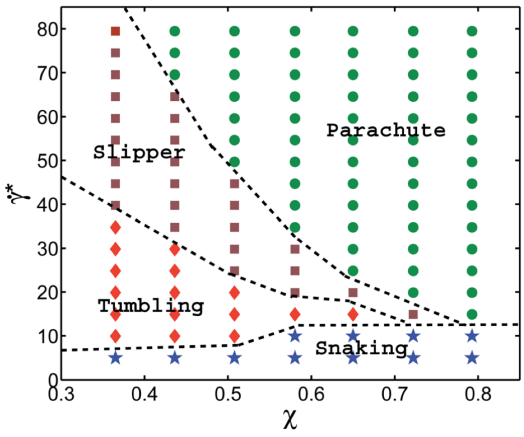

Figure 2: Arrangement of RBCs in Microchannels. Phase diagram for Föppl- von Karman number $\Gamma = K_0 R_0^2/\kappa = 2662$ (with two-dimensional Young modulus $K_0 = 18.9 \times 10^{-6} Nm^{-1}$, $\kappa = 3 \times 10^{-19} J$), which mimics average membrane properties of a healthy RBC. The diagram shows various RBC dynamics states depending on the flow strength characterized by $\dot{\gamma}^*$ and confinement $\chi = R_0/R_{cap}$. The symbols indicate simulated parameters, with the RBC states: parachute (green circles), slipper (brown squares), tumbling (red diamonds) and snaking (blue stars) discocytes. Phase boundaries are shown by dashed lines, which are guides to the eye. From Fedosov et al. (2014b).

2.2 Clustering and Arrangements of Many Red Blood Cells in Microchannel Flows

When several cells in a microcapillary are considered, hydrodynamic interactions are responsible for a strong flow-mediated clustering tendency at low hematocrits (McWhirter et al., 2009, 2011). Beyond a critical flow rate, which is related to the discocyte-to-parachute transi-

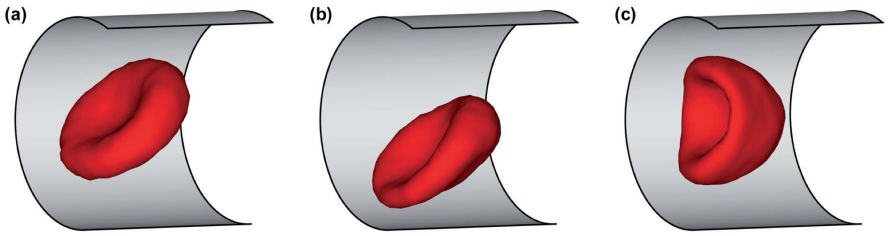

Figure 1: Conformations of a single RBC in Microchannel Flow. Simulation snapshots for confinement $\chi = 0.58$. (a) A biconcave RBC shape at $\dot{\gamma}^* = 5$; (b) an off-center slipper cell shape at $\dot{\gamma}^* = 24.8$; and (c) a parachute shape at $\dot{\gamma}^* = 59.6$. From Fedosov et al. (2014b).

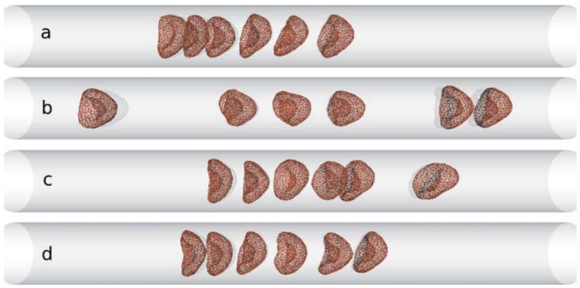

Figure 3: Clustering of RBCs in Microchannels. Sequential snapshots taken during a simulation run with six cells at $g^* = 15.9$ with $L_z/R_0 = 28$ and $R_{cap}/R_0 = 1.58$. (a) $t/\tau = 50$; (b) $t/\tau = 100$; (c) $t/\tau = 150$; and (d) $t/\tau = 200$, where τ is a characteristic RBC relaxation time in equilibrium. From McWhirter et al. (2011).

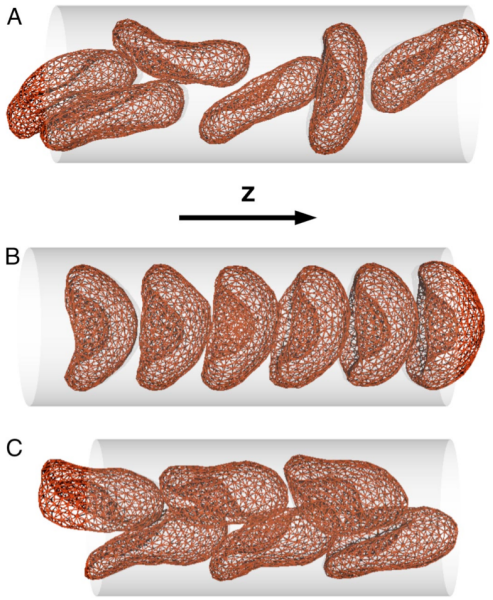

Figure 4: Arrangement of RBCs in Microchannels. Flow simulation for confinement $\chi = R_{cap}/R_0 = 0.714$ with flow from left to right. (A) Disordered-discocyte phase for $H_t = 0.32$ and $v_0^* = 2.5$; (B) Aligned-parachute phase for $H_t = 0.32$ and $v_0^* = 10$. (C) Zigzag-slipper phase for $H_t = 0.37$ and $v_0^* = 10$. From McWhirter et al. (2009).

tion of a single RBC, clusters are the prevalent conformation. These clusters are not permanent, but occasionally break up and reform, see Fig. 3. The stability of clusters is on one hand due to hydrodynamic interactions, which favor a certain distance between RBCs related either to the RBC or the channel diameter, on the other hand due to the stronger deformation of single cells, which makes them move faster in the center of the channel and thereby join the next cluster ahead in the flow direction. The existence of such clusters has been confirmed experimentally (Gaehtgens et al., 1980; Tomaiuolo et al., 2012).

At higher hematocrits, several distinct flow phases are obtained in simulation, such as a disordered arrangement of discocytes, a regular array of parachutes, or a zig-zag arrangement of slippers (McWhirter et al., 2009, 2012), see Fig. 4. Here, the disordered-discocyte phase occurs at relatively small H_t and low flow velocities, the aligned-parachute phase at higher flow velocities, and the zigzag-slipper phase at higher hematocrits. More complex arrangements are found for lower confinements (McWhirter et al., 2012). Similar RBC conformations have been observed experimentally in microvessels (Skalak, 1969) and microcapillaries (Gaehtgens et al., 1980).

2.3 Blood Viscosity

For large vessels, blood behaves like a continuum fluid, which displays a strong shear-thinning behavior (Merrill et al., 1963; Chien et al., 1966; Skalak et al., 1981; Skalak, 1990). Our mesoscale hydrodynamics simulations on the cellular level show quantitatively how this behavior arises from RBC deformability and cell-cell attraction (Fedosov et al., 2011). The simulation results for the viscosity as a function of shear rate are displayed and compared with experimental results in Fig. 5, both for whole blood and for Ringer solution (no attractive interactions between RBCs). For whole blood, there is one adjustable parameter, the strength of the attractive interaction between two RBCs. The comparison of simulation results and experimental data allow us to determine this force strength, which corresponds to a break-up pulling force between two aggregated RBCs in the normal direction in the range of 3.0 to 7.0 pN, and a tangential or sliding break-up force of 1.5 to 3.0 pN. These forces are much smaller than those imposed on single RBCs in stretching tests with optical tweezers (Suresh et al., 2005).

The data in Fig. 5 show that the strong shear-thinning behavior of whole blood at low shear rates is due to the attraction between RBCs, which leads to roleaux formation, and roleaux break-up with increasing shear rate. For shear rates higher than a "critical" shear rate $\dot{\gamma}_c$ of about $5s^{-1}$, roleaux do not play a significant role anymore. The subsequent shear thinning for higher shear rates is due to RBC deformation. This is demonstrated by the asphericity distributions displayed in Fig. 6. For $\dot{\gamma} = 0.045s^{-1} < \dot{\gamma}_c$, RBCs are undeformed discocytes. For $\dot{\gamma} = 45s^{-1} > \dot{\gamma}_c$, in the middle of the second shear-thinning regime, cells become more rounded by forming folded or parachute-like shapes. Finally, for $\dot{\gamma} = 1425s^{-1} \gg \dot{\gamma}_c$, cells are strongly elongated into prolate shapes, and the viscosity has reached its large-shear-rate plateau.

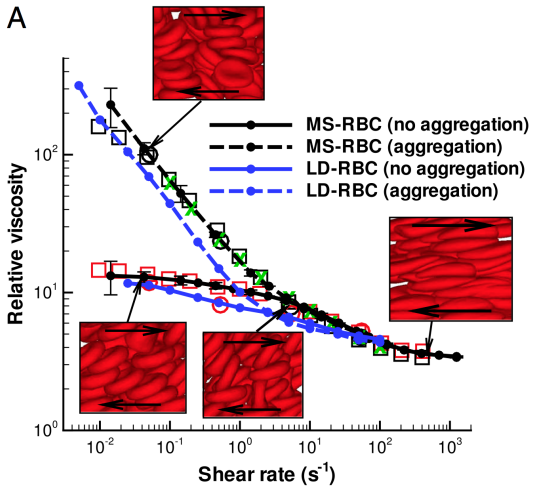

Figure 5: Viscosity of RBCs in Shear Flow. Relative viscosity (the cell suspension viscosity normalized by the solvent viscosity) as a function of shear rate at $H = 45\%$ and 37^oC. Simulation results are shown by curves as indicated, and experimental data are displayed as symbols. Whole blood: green crosses (Merrill et al., 1963); black circles (Chien et al., 1966); black squares (Skalak et al., 1981). Ringer erythrocyte suspension (no attraction): red circles (Chien et al., 1966); red squares (Skalak et al., 1981). From Fedosov et al. (2011).

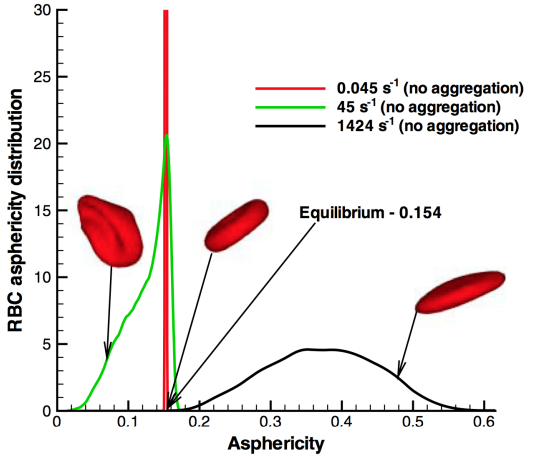

Figure 6: Structural Properties of RBCs in Dense Suspensions under Shear Flow. RBC asphericity distributions characterizing the deviation from a spherical shape as a function of shear rate. The asphericity is defined as $[(\lambda_1-\lambda_2)^2+(\lambda_2-\lambda_3)^2+(\lambda_3-\lambda_1)^2]/(2R_g^4)$, where $\lambda_1 \le \lambda_2 \le \lambda_3$ are the eigenvalues of the gyration tensor and $R_g^2 = \lambda_1+\lambda_2+\lambda_3$. The asphericity for a single RBC in equilibrium is equal to 0.154. From Fedosov et al. (2011).

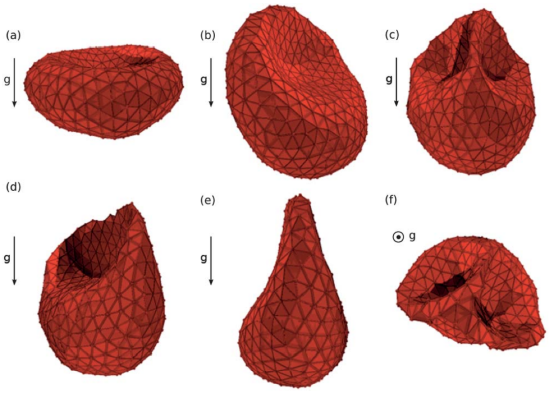

Figure 7: RBC Shapes in Sedimentation. (a) Parachute for $g^* = 2800$ and $\kappa/k_BT = 30$. (b) Teardrop for $g^* = 5600$ and $\kappa/k_BT = 30$. (c) Fin-tailed sphere for $g^* = 21000$ and $\kappa/k_BT = 10$. (d) Asymmetric teardrop for $g^* = 11200$, and $\kappa/k_BT = 20$. (e) Symmetric teardrop for $g^* = 11200$, and $\kappa/k_BT = 40$. (f) The same as (c) but seen from above. Here, g^* is related to the density difference of internal and external fluids. In all cases, the dimensionless shear modulus is $\mu R_0^2/\kappa = 105$. From Peltomäki and Gompper (2013).

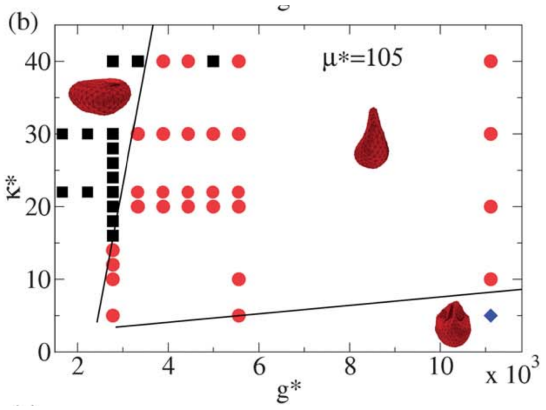

Figure 8: RBC Phase Diagram in Sedimentation. The solid lines, which indicate phase boundaries, are guides to the eye. Here, $\kappa^* = \kappa/k_BT$ and g^* is the dimensionless acceleration related to the density difference of internal and external fluids. From Peltomäki and Gompper (2013).

2.4 Sedimentation

An important medical method to characterize blood properties is sedimentation of blood and the erythrocyte sedimenting rate (ESR), a clinical test regarding blood properties and patient health. We therefore consider the sedimentation of RBCs due to gravitation or centrifugation at low Reynolds numbers. The RBCs are found to assume different shapes depending on the elastic moduli of the cell membranes and the strength of the gravitation; these include parachutes, teardrops, and fin-tailed spheres (Peltomäki and Gompper, 2013), see Fig. 7. The simulation results can be used to construct a phase diagram of the shapes, see Fig. 8. The parachute and tear-drop shapes have been seen experimentally by Hoffman and Inoué (2006), whereas the fin-tailed spheres correspond to the experimental results by Corry and Meiselman (1978) at very high acceleration.

The sedimentation velocity is found to be essentially independent of the cell shape (Peltomäki and Gompper, 2013). Also, RBCs are shown to lack an observable horizontal drift component of the motion even for asymmetric cell shapes. Thus, the clinical erythrocyte sedimentation rate (ESR) is mainly sensitive to attractive interactions among RBCs.

2.5 Margination of White Blood Cells and Drug-Carriers

Due to the overwhelming fraction of RBCs compared to all other cellular components, the flow behavior of blood is dominated by the deformability and interactions of RBCs. However, it is of course very interesting to consider the behavior of white blood cells (WBCs), platelets, large proteins like the von Willebrand factor, and of drug carriers in blood flow. Here, the interaction with RBCs is of crucial importance. The dynamics of RBCs in microcapillaries, in particular their hydrodynamic lift force close to a wall (Sukumaran and Seifert, 2001; Abkarian et al., 2002; Messlinger et al., 2009) and the resulting formation of a red-blood-cell-free layer near the wall (Fåhraeus and Lindqvist, 1931), leads to the margination of other particles, *i.e.* to their increased probability to be localised near the wall. Margination strongly depends on hematocrit and flow rates.

This is demonstrated here for the margination of WBCs. Simulation results for the margination probability – the probability to find the cen-

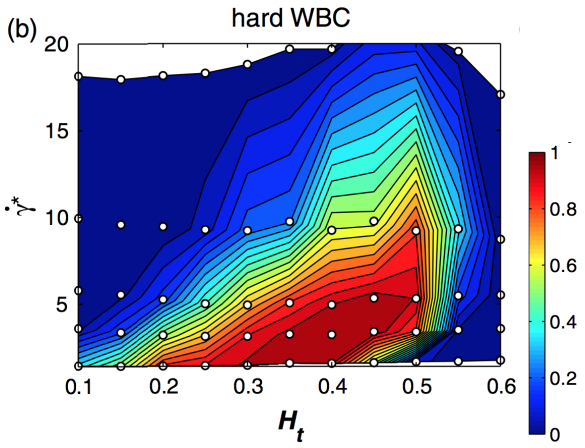

Figure 9: WBC Margination Probability in Microcapillary Flow. Dependence of WBC margination probability on $\dot{\gamma}^*$ and H_t, for a channel of width $W = 20\mu$m in two dimensions. Symbols indicate the simulated parameter values. From Fedosov et al. (2012).

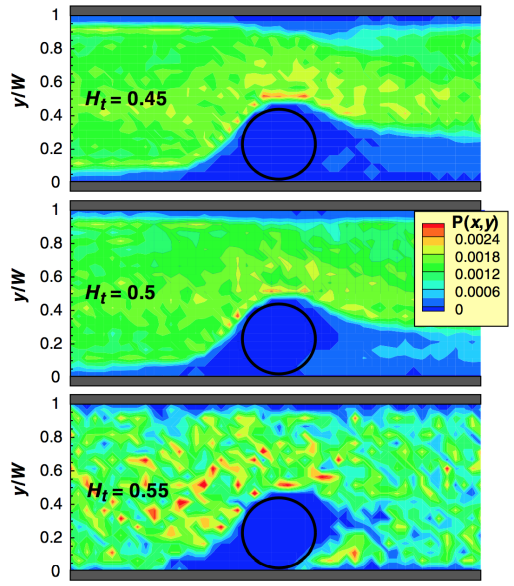

Figure 10: RBC Distribution in WBC Margination. RBC center-of-mass distributions around a marginated hard WBC for various H_t values at $\dot{\gamma}^* = 3.34$. The channel width is $W = 20\mu$m in two spatial dimensions. The circle schematically shows the WBC location. The flow direction is from left to right. From Fedosov et al. (2012).

ter of mass of a WBC in a layer near the surface which is only slightly wider than the WBC radius – are shown in Fig. 9 as a function of hematocrit and pseudo shear rate (Fedosov et al., 2012; Fedosov and Gompper, 2014). With increasing hematocrit, WBCs become increasingly marginated, because RBCs populate the core of the microchannel more densely, and thereby push the WBC to the boundaries. Interestingly, at large hematocrits the inverse behavior is found – the margination probability decreases again. The origin of this effect is illustrated in Fig. 10. At hematocrits smaller than about $H_t = 0.45$, the region in front of the rolling WBC is nearly empty of RBCs, whereas the RBCs colliding with the WBC on its backside push it towards the wall. However, for $H_t \gtrsim 0.50$, the region in front of the WBC begins to fill up with RBCs; since the RBCs near the wall move more slowly than the WBC, they act as a "springboard" which pushes the WBC towards the center of the channel.

Margination is also very important for drug carriers, because their enrichment near the ves-

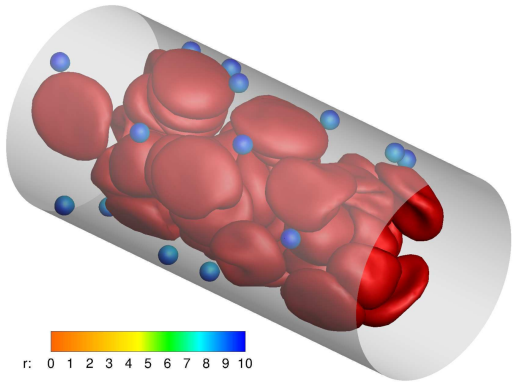

Figure 11: Margination of Drug Carriers in Microchannel Flows. 3D simulations of blood flow for the shear rate of $\dot{\gamma}^* \simeq 60$ and hematocrit $H_t = 0.4$. RBCs are drawn in red, while spherical carriers with a diameter of 1.83μm are colored according to their radial position r, as indicated. For better visibility, carrier positions from several snapshots are superimposed. From Müller et al. (2014).

sel wall helps to increase their effect while keeping the overall drug concentration low. It is therefore interesting for the design of efficient carriers to determine the optimal size (Sanhai et al., 2008). Of course, margination is not the only relevant criterion, but blood circulation time is equally important.

In our simulations study, we focus on the dependence of margination of drug carriers on their size and shape, as an essential precondition of adhesion to the vessel walls (Müller et al., 2014). Two different particle shapes (spherical and ellipsoidal) and various sizes, ranging from about hundred nanometers to several micrometers, are considered. An example is shown in Fig. 11, where the micron-size spherical carriers can be seen to be very well marginated. We find that the margination properties of particles worsen with decreasing carrier size. Spherical particles yield slightly better margination than ellipsoidal particles (Müller et al., 2014); however, adhesion of ellipsoidal carriers is expected to be superior due to a larger area for adhesive interactions (Dasgupta et al., 2014). Thus, micron-size ellipsoidal particles seem to be favorable for drug delivery in comparison to sub-micron particles and sphere-shaped carriers.

Acknowledgments

Dmitry A. Fedosov acknowledges funding by the Alexander von Humboldt Foundation. Kathrin Müller acknowledges support by the International Helmholtz Research School of Biophysics and Soft Matter (IHRS BioSoft). We also gratefully acknowledge CPU-time grants by the Jülich Supercomputing Center.

References

Abkarian, M., Faivre, M., Horton, R., Smistrup, K., Best-Popescu, C. A., Stone, H. A., 2008. Cellular-scale hydrodynamics. Biomed. Mater. 3, 034011.

Abkarian, M., Lartigue, C., Viallat, A., 2002. Tank treading and unbinding of deformable vesicles in shear flow: determination of the lift force. Phys. Rev. Lett. 88, 068103.

Chien, S., Usami, S., Taylor, H. M., Lundberg, J. L., Gregersen, M. I., 1966. Effects of hematocrit and plasma proteins on human blood rheology at low shear rates. J. Appl. Physiol. 21, 81–87.

Corry, W. D., Meiselman, H. J., 1978. Deformation of human erythrocytes in a centrifugal field. Biophys. J. 21, 19–34.

Dasgupta, S., Auth, T., Gompper, G., 2014. Shape and orientation matter for the cellular uptake of nonspherical particles. Nano Lett. 14, 687–693.

Espanol, P., Revenga, M., 2003. Smoothed dissipative particle dynamics. Phys. Rev. E 67, 026705.

Espanol, P., Warren, P. B., 1995. Statistical mechanics of dissipative particle dynamics. Europhys. Lett. 30, 191–196.

Fedosov, D. A., Caswell, B., Karniadakis, G. E., 2010. A multiscale red blood cell model with accurate mechanics, rheology, and dynamics. Biophys. J. 98, 2215–2225.

Fedosov, D. A., Fornleitner, J., Gompper, G., 2012. Margination of white blood cells in microcapillary flow. Phys. Rev. Lett. 108, 028104 [1–5].

Fedosov, D. A., Gompper, G., 2014. White blood cell margination in microcirculation. Soft Matter 10, 2961–2970.

Fedosov, D. A., Noguchi, H., Gompper, G., 2014a. Multiscale modeling of blood flow: From single cells to blood rheology. Biomech. Model. Mechanobiol. 13, 239–258.

Fedosov, D. A., Pan, W., Caswell, B., Gompper, G., Karniadakis, G. E., 2011. Predicting blood rheology in silico. Proc. Natl. Acad. Sci. USA 108, 11772–11777.

Fedosov, D. A., Peltomäki, M., Gompper, G., 2014b. Deformation and dynamics of red blood cells in flow through cylindrical microchannels. Soft Matter 10, 4258–4267.

Fåhraeus, R., Lindqvist, T., 1931. The viscosity of the blood in narrow capillary tubes. Am. J. Phys. 96, 562–568.

Gaehtgens, P., Dührssen, C., Albrecht, K. H., 1980. Motion, deformation, and interaction of blood cells and plasma during flow through narrow capillary tubes. Blood Cells 6, 799–812.

Gompper, G., Ihle, T., Kroll, D. M., Winkler, R. G., 2009. Multi-particle collision dynamics – a particle-based mesoscale simulation approach to the hydrodynamics of complex fluids. Adv. Polym. Sci. 221, 1–87.

Gompper, G., Kroll, D. M., 1997. Network models of fluid, hexatic and polymerized membranes. J. Phys.: Condens. Matter 9, 8795–8834.

Gompper, G., Kroll, D. M., 2004. Triangulated-surface models of fluctuating membranes. In: Nelson, D. R., Piran, T., Weinberg, S. (Eds.), Statistical Mechanics of Membranes and Surfaces, 2nd Edition. World Scientific, Singapore, pp. 359–426.

Hoffman, J. F., Inoué, S., 2006. Directly observed reversible shape changes and hemoglobin stratification during centrifugation of human and amphiuma red blood cells. Proc. Natl. Acad. Sci. USA 103, 2971–2976.

Kaoui, B., Biros, G., Misbah, C., 2009. Why do red blood cells have asymmetric shapes even in a symmetric flow? Phys. Rev. Lett. 103, 188101.

Kaoui, B., Tahiri, N., Biben, T., Ez-Zahraouy, H., Benyoussef, A., Biros, G., Misbah, C., 2011. Complexity of vesicle microcirculation. Phys. Rev. E 84, 041906.

Kapral, R., 2008. Multiparticle collision dynamics: Simulation of complex systems on mesoscales. Adv. Chem. Phys. 140, 89–146.

McWhirter, J. L., Noguchi, H., Gompper, G., 2009. Flow-induced clustering and alignment of red blood cells in microchannels. Proc. Natl. Acad. Sci. USA 106, 6039–6043.

McWhirter, J. L., Noguchi, H., Gompper, G., 2011. Deformation and clustering of red blood cells in microcapillary flows. Soft Matter 7, 10967–10977.

McWhirter, J. L., Noguchi, H., Gompper, G., 2012. Ordering and arrangement of deformed red blood cells in flows through microcapillaries. New J. Phys. 14, 085026 [1–23].

Merrill, E. W., Gilliland, E. R., Cokelet, G., Shin, H., Britten, A., Wells, J. R. E., 1963. Rheology of human blood near and at zero flow. Biophys. J. 3, 199–213.

Messlinger, S., Schmidt, B., Noguchi, H., Gompper, G., 2009. Dynamical regimes and hydrodynamic lift of viscous vesicles under shear. Phys. Rev. E 80, 011901.

Müller, K., Fedosov, D. A., Gompper, G., 2014. Margination of micro- and nano-particles in blood flow and its effect on the efficiency of drug delivery. Sci. Rep. 4, 4871 [1–8].

Noguchi, H., Gompper, G., 2005. Shape transitions of fluid vesicles and red blood cells in capillary flows. Proc. Natl. Acad. Sci. USA 102, 14159–14164.

Peltomäki, M., Gompper, G., 2013. Sedimentation of single red blood cells. Soft Matter 9, 8346–8358.

Sanhai, W. R., Sakamoto, J. H., Canady, R., Ferrari, M., 2008. Seven challenges for nanomedicine. Nat. Nanotechnol. 3, 242–244.

Secomb, T. W., Skalak, R., Özkaya, N., Gross, J. F., 1986. Flow of axisymmetric red blood cells in narrow capillaries. J. Fluid Mech. 163, 405–423.

Skalak, R., 1969. Deformation of red blood cells in capillaries. Science 164, 717–719.

Skalak, R., 1990. Capillary flow: Past, present, and future. Biorheology 27, 277–293.

Skalak, R., Keller, S. R., Secomb, T. W., 1981. Mechanics of blood flow. J. Biomech. Eng. 103, 102–115.

Sukumaran, S., Seifert, U., 2001. Influence of shear flow on vesicles near a wall: A numerical study. Phys. Rev. E 64, 011916.

Suresh, S., Spatz, J., Mills, J. P., Micoulet, A., Dao, M., Lim, C. T., Beil, M., Seufferlein, T., 2005. Connections between single-cell biomechanics and human disease states: gastrointestinal cancer and malaria. Acta Biomaterialia 1, 15–30.

Suzuki, Y., Tateishi, N., Soutani, M., Maeda, N., 1996. Deformation of erythrocytes in microvessels and glass capillaries: effects of erythrocyte deformability. Microcirc. 3, 49–57.

Tomaiuolo, G., Lanotte, L., Ghigliotti, G., Misbah, C., Guido, S., 2012. Red blood cell clustering in poiseuille microcapillary flow. Phys. Fluids 24, 051903.

Tomaiuolo, G., Simeone, M., Martinelli, V., Rotoli, B., Guido, S., 2009. Red blood cell deformation in microconfined flow. Soft Matter 5, 3736–3740.